Lithiation of Silicon Nanoparticles Confined in Carbon Nanotubes

Wan-Jing Yu, Chang Liu,* Peng-Xiang Hou, Lili Zhang, Xu-Yi Shan, Feng Li, and Hui-Ming Cheng*

Shenyang National Laboratory for Materials Science, Institute of Metal Research, Chinese Academy of Sciences, 72 Wenhua Road, Shenyang 110016, China

ABSTRACT Silicon has the highest theoretical lithium storage capacity of all materials at 4200 mAh/g; therefore, it is considered to be a promising candidate as the anode of high-energy-density lithium-ion batteries (LIBs). However, serious volume changes caused by lithium insertion/deinsertion lead to a rapid decay of the performance of the Si anode. Here, a Si nanoparticle (NP)-filled carbon nanotube (CNT) material was prepared by chemical vapor deposition, and a nanobattery was constructed inside a transmission electron microscope (TEM) using the Si NP-filled CNT as working electrode to directly investigate the structural change of the Si NPs and the confinement effect of the CNT during the lithiation and delithiation processes. It is found that the volume expansion (~180%) of the lithiated Si NPs is restricted by the wall of the CNTs and that the CNT can accommodate this volume expansion without breaking its tubular structure. The Si NP-filled CNTs showed a high reversible lithium storage capacity and desirable high rate capability, because the pulverization and exfoliation of the Si NPs confined in CNTs were efficiently prevented. Our results demonstrate that filling CNTs with high-capacity active materials is a feasible way to make high-performance LIB electrode materials, taking advantage of the unique confinement effect and good electrical conductivity of the CNTs.

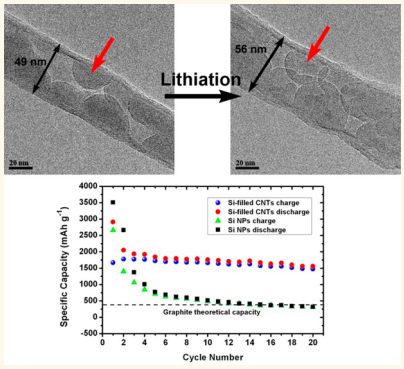

KEYWORDS: lithium-ion batteries · silicon nanoparticles · carbon nanotubes · confinement effect · *in situ* TEM

Rechargeable lithium-ion batteries (LIBs) have attracted great interest in recent years due to their wide range of applications in portable electronic devices and their promise for powering electric vehicles (EVs) and hybrid electric vehicles (HEVs).[1−3] However, the performance of LIBs still needs to be improved to meet the increasing demand for higher energy and power density and longer cycling life. To achieve the above objectives, it is essential to develop novel electrode materials with higher electrochemical performance.[4,5] An attractive candidate for replacing the current carbonaceous anodes is silicon, which has the highest theoretical gravimetric and volumetric capacity of ~4200 mAh g^{-1} and ~8500 mAh cm^{-3} among all possible anode materials.[6−10] However, the major drawback of a silicon electrode is the extremely high volume expansion of ~300% that can occur when lithiation occurs, which leads to mechanical stresses large enough to fracture and severely pulverize the Si electrode and causes the loss of electrical contact and rapid capacity fade upon cycling.[11] Several strategies have been explored in recent years to improve the cyclability of Si-based anodes.[9,12−20] For example, Cui *et al.* prepared Si nanowires and nanoparticles encapsulated in carbon shells with excellent electrochemical performance.[7,21] On the other hand, due to their one-dimensional tubular morphology, good electrical conductivity, high mechanical strength and structural flexibility, and their ability to form an efficient conductive network, carbon nanotubes (CNTs) have drawn intense attention for use as the anode material of LIBs.[22,23] Nanostructures of Si nanobeads strung by CNTs[24] and Si nanotubes confined in CNTs[25] were proposed to accommodate huge volume changes of Si during lithiation and delithiation without appreciable mechanical failure. Most previous reports on CNT-containing Si anode materials mainly emphasized the electrical connection of Si with the CNT exterior surface by simple mechanical mixing,[26] growth of CNTs on Si,[18] anchoring Si on the CNT surface,[27] and deposition of Si on a CNT film to form a Si/CNT composite paper,[28] in which the CNTs function as both a good electrical conducting network and a mechanical support for structural reinforcement. However, the confinement effect of CNTs is not satisfactory due to the inhomogeneous distribution of Si particles and the fact that they are not strongly confined by the CNT

* Address correspondence to (C. Liu) cliu@imr.ac.cn, (H.-M. Cheng) cheng@imr.ac.cn.

Received for review January 9, 2015 and accepted April 13, 2015.

Published online April 13, 2015
10.1021/acsnano.5b00157

network within a nanospace. On the other hand, the detailed reaction process for the above Si/CNT composites and the role that CNTs play during lithiation/delithiation are far from clear. In addition, there is no report revealing the confinement effect of CNTs on active electrode materials, especially an anode in which Si fine particles are filled inside CNTs. However, understanding of this effect may be essential for the design and optimization of high-performance hybrid electrode materials for LIBs.

In this work, we prepared a Si nanoparticle (NP)-filled CNT structure by the chemical vapor deposition of SiH_4 into the hollow cores of CNTs with two open ends. To the best of our knowledge, this is the first report of the synthesis of Si NPs encapsulated in CNTs. A nanobattery was then constructed inside a transmission electron microscope using the Si NP-filled CNT as a working electrode to directly investigate the structural change of Si NPs and the confinement effect of CNTs during lithiation and delithiation. Our results show that CNTs can accommodate the large volume expansion of the lithiated Si NPs. The diameter of the CNTs was observed to expand by 14%, while the overall morphology and hollow tubular structure of the CNTs were preserved without any rupture. Furthermore, the transport velocity of lithium ions along the axis of the CNTs was measured to be ~30 nm/s. Excellent lithium storage properties of the Si NP-filled CNTs in terms of high reversible capacity, good cycling stability, and high rate capability were demonstrated.

RESULTS AND DISCUSSION

Structural Characterization of Si NP-Filled CNTs. Figure 1a and b show typical scanning electron microscopy (SEM) images of the Si NP-filled CNTs with a uniform length of ~30 μm and a diameter of ~50 nm. It can be seen that there is no Si deposited on the outer surface of the CNTs. Figure 1c, a transmission electron microscopy (TEM) image, reveals that the Si NPs are well dispersed inside the hollow core of the CNTs, and the selected area electron diffraction (SAED) pattern (inset of Figure 1c) indicates that they are amorphous.[28] This is in good agreement with the results of laser Raman spectroscopy (Figure S1, Supporting Information)[29,30] and X-ray diffraction (XRD) characterization (Figure S2, Supporting Information). A high-magnification TEM image of a Si NP-filled CNT is shown in Figure 1d. It can be seen that the thickness of the tube wall is ~5 nm, and the Si NPs are firmly anchored onto the inner CNT wall. The walls of the CNT are undulating due to the low synthesis temperature used. No lattice fringes of the Si NPs can be discerned, in good agreement with the Raman, SAED, and XRD characterization results. For better visualization of the Si NP dispersion, a high-angle annular-dark-field (HAADF) image of the Si NP-filled CNTs (Figure 1e) was acquired. The elemental maps of carbon, silicon, and oxygen from the rectangular area

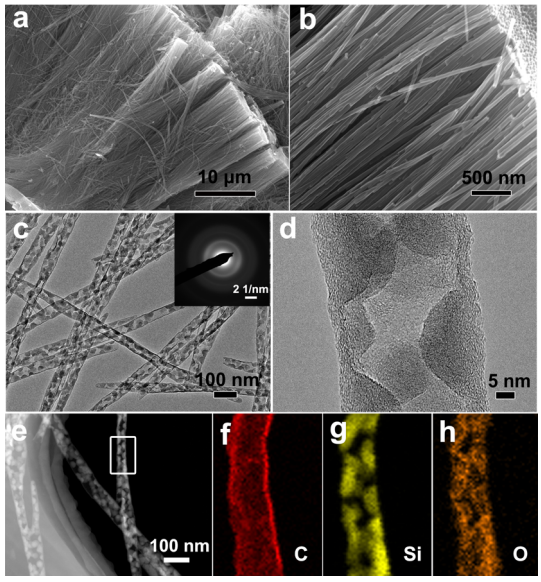

Figure 1. Microstructure and elemental analysis of the Si NP-filled CNTs. (a and b) SEM images; (c) low- and (d) high-magnification TEM images, clearly showing that Si NPs are 100% filled inside the CNTs. The inset in (c) shows the SAED pattern. (e) HAADF image and the corresponding (f) C, (g) Si, and (h) O elemental mapping.

indicated in Figure 1e are shown in Figure 1f, g, and h, respectively. The appearance of oxygen signals can be ascribed to oxygen-containing functional groups on the CNT surface (Figures S3 and S4a, Supporting Information) induced during the chemical removal of the anodic aluminum oxide (AAO) template and partial oxidation of the filled Si NPs. X-ray photoelectron spectroscopy (XPS) analysis (Figure S4b and Table S1, Supporting Information) shows that the atomic percentage of silicon is 22.2% in the Si NP-filled CNTs, much higher than that of oxygen (6.3%).

Nanobattery Construction. *In situ* TEM electrochemical measurements have proven to be a direct and effective way to probe the morphology and structure changes of electrode materials during the discharge/charge process.[31,32] We constructed a nanobattery inside a TEM using a Si NP-filled CNT as the working electrode to examine its structural changes during lithiation/delithiation and to obtain insight into the spatial confinement effect of the CNTs. A schematic construction of the nanobattery is shown in Figure 2a. A Si NP-filled CNT was loaded onto the edge of a gold probe with a freshly cut tip, serving as the working electrode. A small piece of metallic lithium attached to another gold rod was used as the reference/counter electrode. A Li_2O layer on the surface of the Li metal formed by exposure to air for less than 5 s served as a solid electrolyte.[33,34] Figure 2b shows a low-magnification TEM image of a Si NP-filled CNT bridging the electrodes. The lithiation/delithiation experiment was conducted by applying a voltage of −2/+2 V to the working electrode.

Microstructure Characterization. Figure 3 shows TEM images of a Si NP-filled CNT before and after lithium

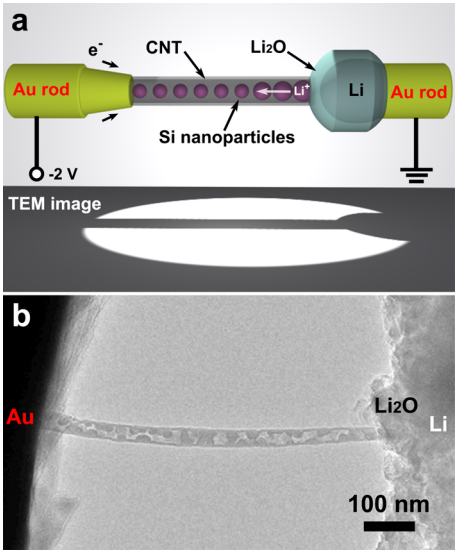

Figure 2. *In situ* TEM electrochemical measurements. (a) Schematic showing the construction of the electrochemical testing setup. (b) TEM image showing a Si NP-filled CNT bridging a Au probe and a Li electrode.

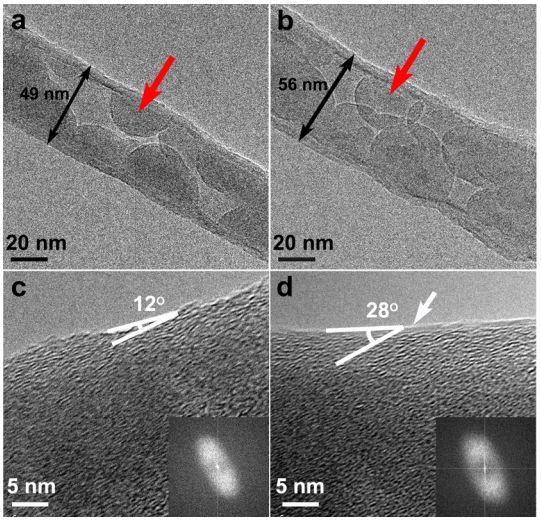

Figure 3. Structural changes of the Si NP-filled CNT before and after lithiation. Low-magnification TEM images of the (a) pristine and (b) lithiated Si NP-filled CNT showing an obvious expansion of both the silicon NPs and the CNT upon lithium insertion. HRTEM images of the Si NP-filled CNT (c) before and (d) after lithiation, showing an increase of the angle between the carbon layers and tube axis after the lithiation. The insets in (c) and (d) are fast Fourier transforms (FFT) of the Si NPs, indicating the existence of amorphous Si and Li_xSi before and after lithiation.

insertion, and the influence of lithiation on the morphology and structure of the Si NPs and CNT is clearly observed. As can be seen in Figure 3a, the pristine Si NPs have a mean diameter of ~20 nm and are firmly attached to the inner wall of the CNT. After lithiation, the size of the Si NPs increased due to the formation of a Li_xSi phase and the accompanying volume expansion (Figure 3b).[35] Typically, a volume expansion of ~180% for the Si NPs (indicated by red arrows) is observed, much less than previously reported results.[33,34,36] This is mainly because the CNT shell confines the expansion of the Li_xSi NPs. The Si NPs are confined in the hollow core of CNTs. As a result, the volume expansion of Si NPs during lithiation is restricted due to the mechanical confinement−lithiation coupling.[37,38] The stress induced by lithiation of Si NPs within CNTs may slow down and limit further lithium diffusion and result in an incomplete lithiation of the encapsulated Si NPs by forming Li_xSi ($x < 3.75$). As a result, a much lower volume expansion rate compared with that of Si existing in a free space was observed.[39,40] Moreover, the thin SiO_x layer on the surface of Si NPs could also contribute to the lower volume expansion.[41] No distinct cracking or pulverization of the lithiated Si NPs was observed, which can be ascribed to their small size and homogeneous volume expansion. It is noteworthy that the lithiated Si NPs maintain good electrical contact with the CNT, as can be observed in Figure 3b. Due to the expansion of the Si NPs and the insertion of lithium ions into the carbon layers, the diameter of the CNT expanded from 49 nm to 56 nm after the electrochemical lithiation, while the hollow tubular structure of the CNT was well preserved and there was no breakage because of its high mechanical strength and good flexibility. These results indicate that CNTs effectively restrain the lithiation-induced swelling and exfoliation of the Si NPs inside them. A TEM image (Figure 3c) of a pristine Si NP-filled CNT shows that most of the carbon layers have an angle of ~12° to the tube axis direction. After lithiation, the angle between the carbon layers and tube axis is obviously increased to ~28°, caused by the volume expansion of the Si NPs and the resulting inhomogeneous stress upon lithiation, which is not observed for the CNTs without filling of Si NPs (Figure S5, Supporting Information). Actually, when the lithiation of the confined Si NPs proceeds, the volume of the Si NPs expands. As a result, a compressive stress is yielded at the radial direction of the CNT. To release this high stress, the CNTs expand locally and an enlarged diameter is observed (Figure 3). Because the CNT has a poor crystallinity and the carbon walls are not quite straight and ordered, the angle between the carbon layers and the tube axis was changed along with the local expansion of the CNT. After delithiation, the stress can be unloaded upon the volume contraction of the Si NPs and the CNT shrinks to its original state. Moreover, the thickness of the CNT wall increased from 4.5 nm to 5.6 nm, possibly due to the insertion of lithium ions. An ultrathin lithium-containing film (marked by a white arrow) related to the solid electrolyte interphase layer in a conventional electrochemical cell has been formed on the outer surface of the CNT (Figure 3d).[42] A fast Fourier transform (FFT) pattern of the Si NPs is shown in the inset of Figure 3c, revealing an amorphous structure of the Si, and no crystalline $Li_{15}Si_4$[10] or $Li_{22}Si_5$[43] was

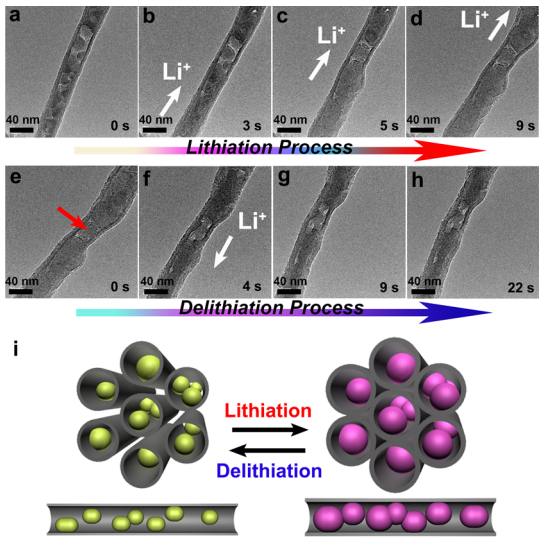

Figure 4. Dynamic structural changes of a Si NP-filled CNT under electrochemical lithiation/delithiation. (a–d) Lithiation of a Si NP-filled CNT. The arrows in images (b)–(d) indicate the Li^+ transport direction and the site where Li_xSi begins to form during lithiation. (e–h) Delithiation of the same Si NP-filled CNT. The arrow in image (f) shows the Li^+ transport direction during delithiation. (i) Illustration of the lithiation/delithiation of Si NP-filled CNTs.

formed after the lithiation (inset of FFT pattern in Figure 3d). This could be ascribed to the lithiation-induced stress and restrained strain in confined space accompanied by the slow-down of Li^+ diffusion, which may lead to a decrease in the equilibrium concentration of Li in the Li–Si phase and the formation of an amorphous lithiated Si structure.[41]

Dynamic Electrochemical Lithiation and Delithiation. Figure 4 depicts dynamic structural evolution of a single Si NP-filled CNT during lithiation/delithiation. When a potential of −2 V was applied, lithiation of the Si NP-filled CNT occurred (Figure 4a–d and Movie S1, Supporting Information). During lithiation, a three-step Li ion transport during the lithiation process is considered. First, Li ions transport through the surface of the CNT. An ultrathin lithium-containing film related to the solid electrolyte interphase layer was observed on the outer surface of the CNTs after lithiation (Figure S5, Supporting Information). A similar phenomenon was also observed for carbon nanofibers (CNFs).[44] Second, since the CNT is poorly crystallized (due to the low synthesis temperature) and the carbon layers are wavy and discontinuous, Li ions can easily penetrate the carbon layer to access the interior of the CNTs. Third, the Si NPs are firmly anchored on the inner surface of the CNTs (Figure 3); thus the Li ions can transport easily through the CNT/Si NP interface to Si NPs by fast surface diffusion, which results in relatively uniform lithiation of the Si NPs.[45] The arrows in Figure 4b–d clearly show the insertion of lithium and the resulting large volume expansion of the Si NPs due to the formation of a Li_xSi phase. While the pristine Si NPs were discontinuously distributed inside the core of the CNT, aggregation of Li_xSi NPs (Figure 4c,d) was observed after lithiation ended. This might be caused by the volume expansion and lithiation-induced contact flattening as a result of the NP deformation through viscous flow, which often happens for particles in a restricted reaction space.[35] The entire lithiation process was finished within 10 s, indicating fast lithium diffusion along the carbon layers and subsequent rapid lithiation of the Si NPs. On the basis of the time delay of the lithiation of the NPs at different locations and the distance of lithium diffusion in Figure 4, we calculated the rate of lithium-ion transport along the CNT to be ~30 nm s^{-1} in the present conditions, which is much higher than that reported for amorphous carbon.[35] Moreover, a lithiation rate of ~20 nm s^{-1} was detected for the Si NPs, much higher than value reported for Si NPs embedded in CNFs.[35] For *in situ* experiments, lithiation behavior can be quite different, relying on different experimental conditions, such as the electrical contact between the sample and Li source, the thickness of the Li_2O layer, and the electric conductivity of the specimen. In this work, the fast lithiation rate demonstrated can be partially ascribed to the small size of the Si NPs, easy breakage of weakened Si–Si bonds induced by partial surface oxidation, the amorphous structure of the NP,[45] and the good contact between the Si NPs and CNTs. No core–shell lithiation of the Si NPs was observed, also indicating a fast lithium transport. Although the internal diameter of the CNT was observed to rapidly increase as a result of the expansion of the Si NPs, there was no cracking, indicating that the CNT has a sufficiently high mechanical strength and good flexibility to accommodate the volume change. Figure 4e–h show the structural change in a lithiated Si NP-filled CNT upon delithiation by reversing the applied bias (Movie S2, Supporting Information). Obviously, the Li_xSi NPs show a uniform contraction during delithiation, accompanied by shrinkage of the CNT diameter. Interestingly, a single lithiated Si particle (indicated by a red arrow in Figure 4e) completely vanished during delithiation, indicating rapid mass transport of Si through viscous flow when Li^+ is removed (indicated by a white arrow in Figure 4f). Finally, an amorphous Si nanorod was preserved inside the core of the CNT. Although the diameter of the CNT was locally enlarged and turned out to be uneven during lithiation (Figure 4c,d) due to the nonuniform distribution of Si NPs filled inside, it can be seen that the morphology and tubular structure of the CNT are well preserved (Figure 4h) after delithiation. By comparing Figure 4g and h, we can see that the delithiation of the Si NP-filled CNT was completed in 9 s, which is exactly the same as that for the lithiation. This means that the dynamics of the insertion and removal of lithium are similar for the Si NP-filled CNTs. This excellent reversibility is very important in improving the high rate capability of the Si NP-filled CNTs. Furthermore, the

growth of an electronically insulating SEI film on the surface of the Si NPs can be effectively hindered during the charge/discharge process due to the shielding of the CNT wall (Figure 3b).[21] Further discharge/charge testing (Figure S6, Supporting Information) showed that the lithiation and delithiation behaviors of the Si NP-filled CNT remained almost unchanged, and during these cycles the morphology and tubular structure of the CNT were well retained.

The overall lithiation/delithiation of the Si NPs confined within a CNT are schematically described in Figure 4i. Upon lithiation, Li ions from the counter electrode can easily enter CNTs through structural defects on the walls or open ends[46,47] and are quickly transported along the tube axis.[21] The Si NPs quickly swell upon the insertion of Li ions. No fracture of Si NPs occurs, due to the spatial restraint of the CNT and the fine Si particle size as well as alleviation of the lithiation-induced strain at the reaction front from two-phase lithiation of the two-step lithiation process in a-Si.[33,40,44] The CNT with good toughness would expand accordingly driven by the stress in the radial direction, caused by lithiation-induced volume expansion of Si, and the diameter of the CNT is increased to partially release the lithiation-induced stress and accommodate the Si volume expansion, which can be well confined inside the nanochannel of the CNT. Meanwhile, the contact area between Si-based NPs and carbon layers greatly increases, which facilitates fast electron transport, and the carbon layers act as a current collector for the encapsulated Si NPs. After delithiation, the NPs show volume shrinkage as a result of the extraction of Li ions from the Li_xSi phase. Simultaneously, the CNT unloads elastically following the volume contraction of Si, which can induce the reversal of hoop stress from the initial tension to compression, leading to the shrinkage of the CNT, and the hollow tubular structure of the CNT was well preserved with the Si restrained inside the core, indicating an excellent stability of this hybrid structure.

Bending and Restoration. An important reason that accounts for the rapid capacity fade of a Si electrode is that the lithiated Si tends to be pulverized and detached from the current collector, due to the large stress caused by volume changes. To further reveal the structural stability of the lithiated Si NP-filled CNTs, we performed compressive loading and unloading tests inside the TEM (Movie S3, Supporting Information). Two lithiated Si NP-filled CNTs marked "1" and "2" in Figure 5a were pushed and pulled using the piezomanipulator of a TEM-scanning tunneling microscopy (STM) holder, and a series of snapshots showing the structural change are given in Figure 5. When a compressive force was applied, the lithiated CNTs were deformed and bent as indicated by the white and black arrows in Figure 5b. Obtuse angles were formed at the bends when the CNTs were continuously driven by the

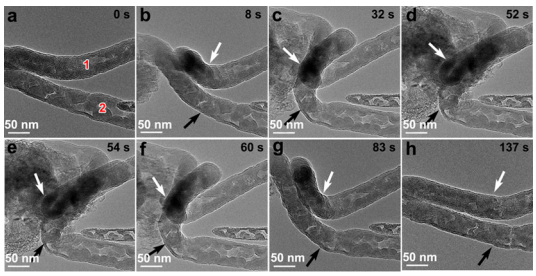

Figure 5. Compressive loading and unloading tests of the lithiated Si NP-filled CNTs. (a–d) Structure of the lithiated Si NP-filled CNTs under compressive loading. (e–h) Structure of the lithiated Si NP-filled CNTs when they are restored to the original position. The white arrows in (b)–(h) show a bend in the upper CNT marked "1". The black arrows in (b)–(h) indicate a bend in the lower CNT marked "2".

piezomanipulator (Figure 5c), and an inverted "S" shape was observed for CNT 2 (Figure 5d). No cracking or fracture appears even at the most sharply bent sites (Figure 5b–d). After compressive loading, the lithiated Si NP-filled CNTs were pulled back to their original positions, as shown in Figure 5h. The CNTs recovered their original straight morphology, and the large deformation at the bends (Figure 5e–h) was fully recovered after unloading without leaving any damage. These bending and pulling tests prove that the Si NP-filled CNTs are strong and flexible enough to undergo reversible deformation. Furthermore, the lithiated Li_xSi NPs are firmly attached to the inner surface of the CNTs during the whole mechanical testing process. These results indicate the strong binding between Si NPs and CNTs, which facilitates the cyclic stability of the Si NP-filled CNTs as an anode material for LIBs.

Electrochemical Performance. We investigated the electrochemical lithium storage performance of the Si NP-filled CNTs as the anode of LIBs. Figure 6a shows differential capacity curves of the first three cycles of Si NP-filled CNTs, which are consistent with typical amorphous silicon charge–discharge behavior.[27,48,49] During the first discharge, one broad and three sharp peaks can be observed. The broad peak at 0.8–0.9 V (*versus* Li/Li^+) is attributed to the side reaction related to the formation of a solid electrolyte interphase (SEI) layer,[28,50] which disappeared in the subsequent discharge process (inset of Figure 6a). The sharp reduction peaks at 0.2, 0.05, and 0.14 V can be assigned to typical lithiation of amorphous silicon[27,48] and Li ion intercalation into the CNTs,[51] respectively. Meanwhile, the peak for the reduction of SiO_x by lithium was not observed,[15,52] possibly due to the very small amount of the SiO_x layer. Two oxidation peaks at around 0.32 and 0.51 V in the first cycle were observed, which can be ascribed to the phase transition between the amorphous Li_xSi alloy phase and the formation of amorphous Si by the dealloying reaction.[27,48] In the subsequent two cycles, the two cathodic peaks during discharge shifted to higher potentials of ~0.22 and

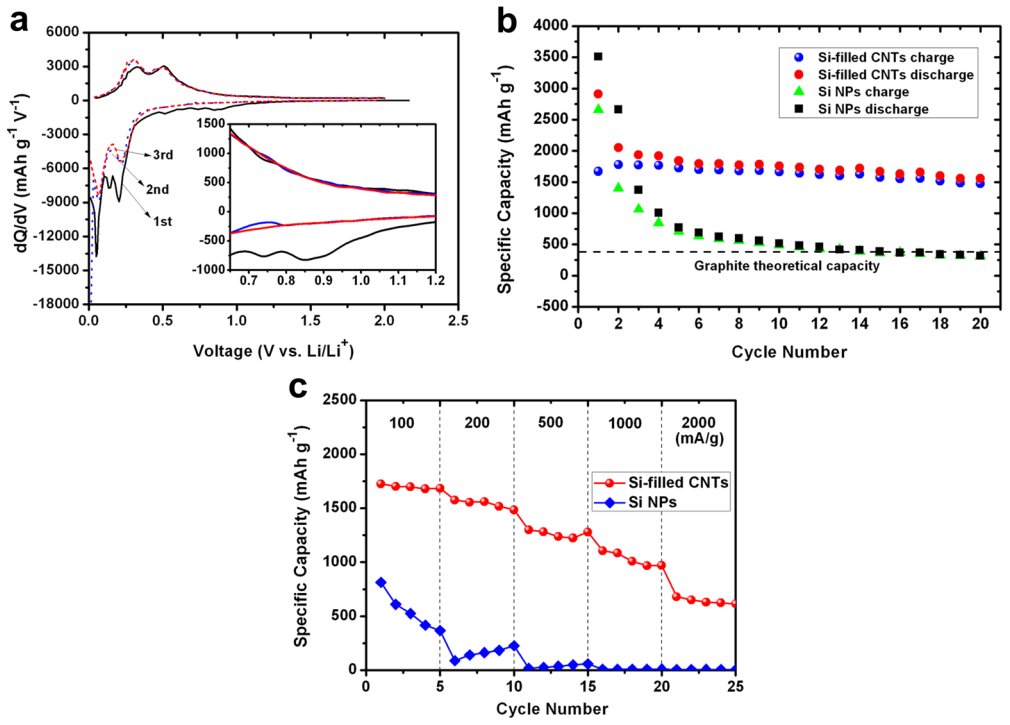

Figure 6. Electrochemical performance of the Si NP-filled CNTs. (a) Plots of the differential capacity of the Si NP-filled CNTs in the first three cycles. The inset in (a) shows the enlargement of a particular potential region. (b) Cycling performance of the Si NP-filled CNTs and that of commercial Si NPs for comparison. (c) Rate performance of the Si NP-filled CNTs and commercial Si NPs.

~0.07 V, while the two anodic peaks during charge downshifted 0.02 V to ~0.3 and ~0.49 V, indicating improved reactivity of the electrodes as a result of the first irreversible Li ion intercalation.[53] Importantly, the peak intensities of the Si NP-filled CNTs remained almost unchanged, showing greatly improved cycling stability. The discharge/charge capacities as a function of cycle number for the Si NP-filled CNTs and commercial Si NPs are shown in Figure 6b. It can be seen that a high reversible capacity of 2660 mA h g^{-1} for the commercial Si NPs was observed (Figure S7, Supporting Information) in the first cycle, but only 311 mA h g^{-1} was delivered after 20 cycles, which is lower than the theoretical capacity of graphite. On the other hand, the reversible specific capacity of the Si NP-filled CNTs is 1671 mA h g^{-1} based on the mass of the composite anode in the initial cycle, and the capacity tends to be stable throughout the whole cycling process. After 20 cycles, the Si NP-filled CNTs retain a reversible capacity of 1475 mA h g^{-1}, which is about 4 times the theoretical capacity of graphite anodes. Figure 6c shows the rate performance (obtained after three initial cycles at a current rate of 50 mA g^{-1}) of the Si NP-filled CNTs and commercial Si NPs. It can be seen that the specific capacity of Si NPs drops rapidly from 813 mAh g^{-1} to 366.9 mAh g^{-1} at a low current density of 100 mA g^{-1} and is only 5.3 mAh g^{-1} at 2000 mA g^{-1}, showing poor rate capability. In contrast, the Si NP-filled CNTs exhibit a high reversible capacity of 1684.1 mAh g^{-1} at 100 mA g^{-1} and more than 1200 mAh g^{-1} at 500 mAh g^{-1}, which is much higher than the value previously reported for Si NPs in CNFs.[54] Remarkably, when the current density is increased to 2000 mA g^{-1} stepwise, the Si NP-filled CNTs still retain a reversible capacity of 614.6 mAh g^{-1}, much higher than the theoretical capacity of graphite. As mentioned above, all these results can be attributed to the unique spatial confinement effect, good electrical conductivity, and excellent mechanical properties of the Si NP-filled CNTs.

General Discussions. CNTs have been widely used as an additive in the electrode materials of LIBs. It is generally considered that the one-dimensional CNTs may form networks and hence improve the electrical conductivity and high rate capability of LIBs. In this study, by fabricating Si NP-filled CNTs and constructing a nanobattery, we clearly demonstrated that CNTs can also improve the ionic conductivity of the electrodes. This is because CNTs have cylindrical sp^2-bonded tube walls, along which Li^+ can transport rapidly.[52] In addition, structural defects in CNTs allow penetration of Li^+ through the tube wall to the hollow core of CNTs. As a result, the ionic conductivity of CNTs is much higher than that of CNFs, in which no "expressway" for Li^+ transport is provided. Another point is that the Si nanoparticles are firmly anchored to the inner wall of the CNTs, which also improves Li^+ transport through the C/Si interface. The Si NPs with a small and uniform size confined in CNTs lead to shortened electronic and ionic transport lengths, which facilitates fast lithium insertion into the Si NPs. Last, but certainly not least,

the confined conductive CNT interior environment can act as a buffer to alleviate volume changes during charge/discharge processes and meanwhile confine Li^+ transport within the CNTs, which can accelerate Li^+ diffusion and lithiation of the Si.

When Si NPs are confined in the nanospace of CNTs, their volume expansion during the lithiation process can be restricted by mechanical confinement of CNTs. During the lithiation, the Si NPs inside CNTs start to swell, which can drive the carbon wall of the CNTs outward to release partial stress from lithiation-induced volume expansion of lithiated Si. Also, compressive stress on lithiated Si from the CNTs is increased together with the expansion of CNTs, due to their elastic feature. Then, the confinement−lithiation coupling can occur, caused by lithiation-induced stress and restrained strain in a confined space, and limiting behavior of deep lithiation in Si could happen due to the slow-down of Li^+ diffusion. Hence, the volume expansion of lithiated Si can be well confined inside the nanochannel of a CNT. Although superior electrochemical Li storage properties of the Si NP-filled CNTs have been achieved, slight performance decay is observed upon cycling compared with some Si-CNT nanocomposite systems.[25,27] This can be ascribed to the instability of the whole electrode structure, which comprises both active and inactive materials, such as Si NP-filled CNTs, Super P carbon, and polyvinylidene fluoride (PVDF) binder. Due to the obvious swelling of the CNTs during lithiation, cracking, deformation, and partial exfoliation of the electrode components may occur upon cycling, leading to deteriorated cycling performance. There are several possible ways to address the above issue. First, the filling rate of Si in CNTs can be properly reduced to improve the structural stability of the electrode. Second, increasing the thickness of the carbon wall of CNTs can further confine the volume expansion in a smaller range. Third, a proper design of the composition and structure of the whole electrode may also further improve its overall electrochemical performance.

CONCLUSION

In summary, a Si NP-filled CNT anode material has been synthesized. Silicon NPs with a mean diameter of ~20 nm were homogeneously encapsulated within the hollow core of the CNTs. Lithiation of individual Si NP-filled CNTs was investigated for the first time by constructing a nanobattery in a transmission electron microscope. The Si NPs inside the CNT were transformed to Li_xSi upon lithiation accompanied by a volume expansion of only ~180%. The CNTs acted as an excellent buffer to accommodate the volume expansion of Si NPs confined in them, and the diameters of the CNTs were increased by ~14%. The lithiation of Si NPs was found to be significantly accelerated inside the CNT because of the good electronic and ionic conductivity of the CNTs, as well as the small size of the Si. The hollow tubular structure of the CNTs was well preserved after lithiation/delithiation tests due to the excellent mechanical strength and flexibility of the CNTs. As an anode of LIBs, the Si NP-filled CNTs exhibited a high reversible lithium storage capacity, good cycling stability, and superior rate capability. Our results indicate that high-performance hybrid electrode materials can be designed and fabricated by optimizing their structure and the combination of materials used.

METHODS

The preparation process of the Si NP-filled CNTs is schematically given in Figure S8 of the Supporting Information.

Synthesis of CNTs by the Anodic Aluminum Oxide Template Method. AAO templates with a channel size of 50 nm were prepared by the two-step anodic oxidation of high-purity aluminum sheets under a direct current (dc) in an acidic solution. The aluminum sheets were sonicated in acetone to degrease them and then etched in a 5 M NaOH aqueous solution to remove impurities and the oxide layer on the surface. They were then anodized under 40 V dc for 4 h in a 3 wt % oxalic acid solution to obtain a nanoporous alumina layer. After removal of the original alumina layer, an ordered pore arrangement was prepared on the Al substrate by the same anodic oxidation treatment described above. Free-standing AAO films with two open ends were obtained by detaching the AAO nanoporous layers from the Al substrates under a dc voltage 5 V higher than the forming voltage in a solution of mixed perchloric acid and acetone. The as-obtained free-standing AAO films were placed in the middle of a quartz tube, which was inserted into a vertical tubular furnace, then heated to 650 °C at a rate of 10 °C min^{-1} under an argon flow of 300 cm^3 min^{-1}. Acetylene was introduced into the furnace at 10 cm^3 min^{-1} with an argon flow of 190 cm^3 min^{-1} as the carrier gas to deposit carbon on the inner surface of the AAO channels. After 2 h of deposition, the acetylene flow was turned off, and the furnace was cooled to room temperature while protected with an Ar flow. As a result, CNTs replicated from the nanochannels of AAO templates were obtained.

Synthesis of Si NPs-Filled CNTs. The Si NP-filled CNTs were prepared by the chemical vapor decomposition of SiH_4 in CNT cores. The AAO film with a deposited carbon layer was placed in the middle of a horizontal tube furnace and heated to 500 °C in 30 min under a hydrogen flow of 200 cm^3 min^{-1}. A SiH_4 (10% SiH_4 in H_2) flow was introduced into the furnace at 10 cm^3 min^{-1} using a hydrogen flow of 40 cm^3 min^{-1} as carrier gas. The CVD process lasted for 20 min. Finally, Si NP-filled CNTs were obtained by dissolving the AAO films in a 10 wt % H_3PO_4 aqueous solution at 60 °C for 24 h.

Structure Characterization. The morphology and microstructure of the samples were observed using scanning (FEI Nova Nano 430 system) and transmission electron microscopes (JEOL JEM-2010 and FEI Tecnai F20). Laser Raman measurements were performed using a Raman spectrometer (Jobin Yvon LabRam HR800) with an excitation laser wavelength of 632.8 nm. X-ray diffraction was used to identify the sample using a diffractometer (Rigaku D/max-2400) with Cu Kα (λ = 1.540 56 Å) radiation. X-ray photoelectron spectroscopy measurements were carried out on an ESCALAB 250 with Al Kα radiation (15 kV, 150 W).

Electrochemical Property Measurements. The electrochemical measurements were carried out with coin-type two-electrode half-cells. To prepare the working electrode, 70 wt % of the Si NP-filled CNTs, 15 wt % conducting agent (Super P), and 15 wt %

polyvinylidene fluoride dissolved in *N*-methyl-2-pyrrolidone were mixed to form a slurry, which was coated on a copper foil and then dried under vacuum at 120 °C for 12 h. Metallic lithium foil was used as the counter/reference electrodes, and a Celgard 2400 membrane was used as separator. $LiPF_6$ (1 M) dissolved in a 1:1 (v/v) mixture of ethylene carbonate and dimethyl carbonate was used as electrolyte. Galvanostatic charge and discharge measurements were carried out in the voltage range 0.01−2.0 V *versus* Li^+/Li at a current density of 100 mA g^{-1} using a battery test system (LAND CT2001A model, Wuhan Jinnuo Eletronic Co. Ltd.)

Construction of the Nanobattery. *In situ* transmission electron microscopy tests were conducted in a Tecnai F20 TEM with a Nanofactory TEM-STM holder. Briefly, the Si NP-filled CNTs were attached to a gold rod by directly touching the sample powder with a freshly cut tip. One protruding Si NP-filled CNT was selected under TEM as the working electrode. A small piece of lithium foil was scratched with another gold rod inside a glovebox filled with argon (O_2 and H_2O content <0.1 ppm) and served as the reference electrode and lithium source. A naturally grown Li_2O layer was formed on the surface of the lithium foil by air exposure (~5 s) and used as the solid electrolyte for Li^+ transport between the Si NP-filled CNT and the metallic Li counter electrode. The counter electrode was mounted on a piezomanipulator and driven to approach the working electrode inside the TEM for the lithiation treatment during the experiment. A potential of −2/+2 V was applied to the Si NP-filled CNT with respect to the Li counter electrode to promote lithiation/delithiation of the samples.

Conflict of Interest: The authors declare no competing financial interest.

Supporting Information Available: Illustration of the preparation of the Si NP-filled CNTs; Raman spectra, XRD patterns, XPS analysis, and SEM images of Si nanomaterials; elemental mapping and TEM images of the CNT; TEM images of a Si NP-filled CNT during multiple lithiation−delithiation cycles; movies showing the microstructural evolution of a Si NP-filled CNT during lithiation and delithiation, as well as a movie of compression and tension tests of a lithiated Si NP-filled CNT. This material is available free of charge *via* the Internet at http://pubs.acs.org.

Acknowledgment. This work was supported by the Ministry of Science and Technology of China (Grants 2011CB932601 and 2011CB932604), National Natural Science Foundation of China (Grants 51221264, 51272257, and 51102242), and Key Research Program of Chinese Academy of Sciences (Grant KGZD-EW-T06).

REFERENCES AND NOTES

1. Tarascon, J. M.; Armand, M. Issues and Challenges Facing Rechargeable Lithium Batteries. *Nature* **2001**, *414*, 359–367.
2. Bruce, P. G.; Scrosati, B.; Tarascon, J. M. Nanomaterials for Rechargeable Lithium Batteries. *Angew. Chem., Int. Ed.* **2008**, *47*, 2930–2946.
3. Jeong, G.; Kim, Y. U.; Kim, H.; Kim, Y. J.; Sohn, H. J. Prospective Materials and Applications for Li Secondary Batteries. *Energy Environ. Sci.* **2011**, *4*, 1986–2002.
4. Liu, C.; Li, F.; Ma, L. P.; Cheng, H. M. Advanced Materials for Energy Storage. *Adv. Mater.* **2010**, *22*, E28–E62.
5. Cheng, F.; Liang, J.; Tao, Z.; Chen, J. Functional Materials for Rechargeable Batteries. *Adv. Mater.* **2011**, *23*, 1695–1715.
6. Boukamp, B. A.; Lesh, G. C.; Huggins, R. A. All-Solid Lithium Electrodes With Mixed-Conductor Matrix. *J. Electrochem. Soc.* **1981**, *128*, 725–729.
7. Chan, C. K.; Peng, H.; Liu, G.; McIlwrath, K.; Zhang, X. F.; Hugins, R. A.; Cui, Y. High-Performance Lithium Battery Anodes Using Silicon Nanowires. *Nat. Nanotechnol.* **2008**, *3*, 31–35.
8. Zhang, S.; Du, Z.; Lin, R.; Jiang, T.; Liu, G.; Wu, X.; Weng, D. Nickel Nanocone-Array Supported Silicon Anode for High-Performance Lithium-Ion Batteries. *Adv. Mater.* **2010**, *22*, 5378–5382.
9. Cao, F. F.; Deng, J. W.; Xin, S.; Ji, H. X.; Schmidt, O. G.; Wan, L. J.; Guo, Y. G. Cu-Si Nanocable Arrays as High-Rate Anode Materials for Lithium-Ion Batteries. *Adv. Mater.* **2011**, *23*, 4415–4420.
10. Wang, C. M.; Li, X.; Wang, Z.; Xu, W.; Liu, J.; Gao, F.; Kovarik, L.; Zhang, J. G.; Howe, J.; Burton, D. J.; *et al*. *In Situ* TEM Investigation of Congruent Phase Transition and Structural Evolution of Nanostructured Silicon/Carbon Anode for Lithium Ion Batteries. *Nano Lett.* **2012**, *12*, 1624–1632.
11. Szczech, J. R.; Jin, S. Nanostructured Silicon for High Capacity Lithium Battery Anodes. *Energy Environ. Sci.* **2011**, *4*, 56–72.
12. Ng, S. H.; Wang, J.; Wexler, D.; Konstantinov, K.; Guo, Z. P.; Liu, H. K. Highly Reversible Lithium Storage in Spheroidal Carbon-Coated Silicon Nanocomposites as Anodes for Lithium-Ion Batteries. *Angew. Chem., Int. Ed.* **2006**, *45*, 6896–6899.
13. Shu, J.; Li, H.; Yang, R.; Shi, Y.; Huang, X. Cage-like Carbon Nanotubes/Si Composite as Anode Material for Lithium Ion Batteries. *Electrochem. Commun.* **2006**, *8*, 51–54.
14. Ma, H.; Cheng, F.; Chen, J. Y.; Zhao, J. Z.; Li, C. S.; Tao, Z. L.; Liang, J. Nest-like Silicon Nanospheres for High-Capacity Lithium Storage. *Adv. Mater.* **2007**, *19*, 4067–4070.
15. Hu, Y. S.; Demir-Cakan, R.; Titirici, M. M.; Muller, J. O.; Schlogl, R.; Antonietti, M.; Maier, J. Superior Storage Performance of a Si@SiOx/C Nanocomposite as Anode Material for Lithium-Ion Batteries. *Angew. Chem., Int. Ed.* **2008**, *47*, 1645–1649.
16. Kim, H. J.; Han, B. H.; Choo, J. B.; Cho, J. Three-Dimensional Porous Silicon Particles for Use in High-Performance Lithium Secondary Batteries. *Angew. Chem., Int. Ed.* **2008**, *47*, 10151–10154.
17. Cui, L. F.; Yang, Y.; Hsu, C. M.; Cui, Y. Carbon-Silicon Core-Shell Nanowires as High Capacity Electrode for Lithium Ion Batteries. *Nano Lett.* **2009**, *9*, 3370–3374.
18. Gao, P.; Nuli, Y.; He, Y. S.; Wang, J.; Minett, A. I.; Yang, J.; Chen, J. Direct Scattered Growth of MWNT on Si for High Performance Anode Material in Li-Ion Batteries. *Chem. Commun.* **2010**, *46*, 9149–9151.
19. Magasinski, A.; Dixon, P.; Hertzberg, B.; Kvit, A.; Ayala, J.; Yushin, G. High-Performance Lithium-Ion Anodes Using a Hierarchical Bottom-Up Approach. *Nat. Mater.* **2010**, *9*, 353–358.
20. Gohier, A.; Laik, B.; Kim, K. H.; Maurice, J. L.; Pereira-Ramos, J. P.; Cojocaru, C. S.; Van, P. T. High-Rate Capability Silicon Decorated Vertically Aligned Carbon Nanotubes for Li-Ion Batteries. *Adv. Mater.* **2012**, *24*, 2592–2597.
21. Liu, N.; Wu, H.; McDowell, M. T.; Yao, Y.; Wang, C.; Cui, Y. A Yolk-Shell Design for Stabilized and Scalable Li-Ion Battery Alloy Anodes. *Nano Lett.* **2012**, *12*, 3315–3321.
22. Zhang, H.; Cao, G.; Yang, Y. Carbon Nanotube Arrays and Their Composites for Electrochemical Capacitors and Lithium-Ion Batteries. *Energy Environ. Sci.* **2009**, *2*, 932–943.
23. Landi, B. J.; Ganter, M. J.; Cress, C. D.; DiLeo, R. A.; Raffaelle, R. P. Carbon Nanotubes for Lithium Ion Batteries. *Energy Environ. Sci.* **2009**, *2*, 638–654.
24. Sun, C. F.; Karki, K.; Jia, Z.; Liao, H.; Zhang, Y.; Li, T.; Qi, Y.; Cumings, J.; Rubloff, G. W.; Wang, Y. A Beaded-String Silicon Anode. *ACS Nano* **2013**, *7*, 2717–2724.
25. Hertzberg, B.; Alexeev, A.; Yushin, G. Deformations in Si−Li Anodes upon Electrochemical Alloying in Nano-Confined Space. *J. Am. Chem. Soc.* **2010**, *132*, 8548–8549.
26. Zhang, Y.; Zhang, X. G.; Zhang, H. L.; Zhao, Z. G.; Li, F.; Liu, C.; Cheng, H. M. Composite Anode Material of Silicon/Graphite/Carbon Nanotubes for Li-Ion Batteries. *Electrochim. Acta* **2006**, *51*, 4994–5000.
27. Wang, W.; Kumta, P. N. Nanostructured Hybrid Silicon/Carbon Nanotube Heterostructures: Reversible High-Capacity Lithium-Ion Anodes. *ACS Nano* **2010**, *4*, 2233–2241.
28. Chou, S. L.; Zhao, Y.; Wang, J. Z.; Chen, Z. X.; Liu, H. K.; Dou, S. X. Silicon/Single-Walled Carbon Nanotube Composite Paper as a Flexible Anode Material for Lithium Ion Batteries. *J. Phys. Chem. C* **2010**, *114*, 15862–15867.

29. Sirenko, A. A.; Fox, J. R.; Akimov, I. A.; Xi, X. X.; Ruvimov, S.; Liliental-Weber, Z. *In Situ* Raman Scattering Studies of the Amorphous and Crystalline Si Nanoparticles. *Solid State Commun.* **2000**, *113*, 553–558.
30. Pollak, E.; Salitra, G.; Baranchugov, V.; Aurbach, D. *In Situ* Conductivity, Impedance Spectroscopy, and ex Situ Raman Spectra of Amorphous Silicon during the Insertion/Extraction of Lithium. *J. Phys. Chem. C* **2007**, *111*, 11437–11444.
31. Liu, X. H.; Huang, J. Y. *In Situ* TEM Electrochemistry of Anode Materials in Lithium Ion Batteries. *Energy Environ. Sci.* **2011**, *4*, 3844–3860.
32. Liu, X. H.; Liu, Y.; Kushima, A.; Zhang, S.; Zhu, T.; Li, J.; Huang, J. Y. *In Situ* TEM Experiments of Electrochemical Lithiation and Delithiation of Individual Nanostructures. *Adv. Energy Mater.* **2012**, *2*, 722–741.
33. Liu, X. H.; Zhong, L.; Huang, S.; Mao, S. X.; Zhu, T.; Huang, J. Y. Size-Dependent Fracture of Silicon Nanoparticles during Lithiation. *ACS Nano* **2012**, *6*, 1522–1531.
34. Liu, X. H.; Zheng, H.; Zhong, L.; Huang, S.; Karki, K.; Zhang, L. Q.; Liu, Y.; Kushima, A.; Liang, W. T.; Wang, J. W.; *et al*. Anisotropic Swelling and Fracture of Silicon Nanowires during Lithiation. *Nano Lett.* **2011**, *11*, 3312–3318.
35. Gu, M.; Li, Y.; Li, X.; Hu, S.; Zhang, X.; Xu, W.; Thevuthasan, S.; Baer, D. R.; Zhang, J. G.; Liu, J.; *et al*. *In Situ* TEM Study of Lithiation Behavior of Silicon Nanoparticles Attached to and Embedded in a Carbon Matrix. *ACS Nano* **2012**, *6*, 8439–8447.
36. Liu, X. H.; Zhang, L. Q.; Zhong, L.; Liu, Y.; Zheng, H.; Wang, J. W.; Cho, J. H.; Dayeh, S. A.; Picraux, S. T.; Sullivan, J. P.; *et al*. Ultrafast Electrochemical Lithiation of Individual Si Nanowire Anodes. *Nano Lett.* **2011**, *11*, 2251–2258.
37. Liu, X. H.; Fan, F.; Yang, H.; Zhang, S.; Huang, J. Y.; Zhu, T. Self-Limiting Lithiation in Silicon Nanowires. *ACS Nano* **2013**, *7*, 1495–1503.
38. Zhang, L. Q.; Liu, X. H.; Liu, Y.; Huang, S.; Zhu, T.; Gui, L.; Mao, S. X.; Ye, Z. Z.; Wang, C. M.; Sullivan, J. P.; *et al*. Controlling the Lithiation-Induced Strain and Charging Rate in Nanowire Electrodes by Coating. *ACS Nano* **2011**, *5*, 4800–4809.
39. McDowell, M. T.; Lee, S. W.; Wang, C.; Cui, Y. The Effect of Metallic Coatings and Crystallinity on the Volume Expansion of Silicon During Electrochemical Lithiation/Delithiation. *Nano Energy* **2012**, *1*, 401–410.
40. Wang, J. W.; He, Y.; Fan, F.; Liu, X. H.; Xia, S.; Liu, Y.; Harris, C. T.; Li, H.; Huang, J. Y.; Mao, S. X.; *et al*. Two-Phase Electrochemical Lithiation in Amorphous Silicon. *Nano Lett.* **2013**, *13*, 709–715.
41. McDowell, M. T.; Lee, S. W.; Ryu, I.; Wu, H.; Nix, W. D.; Choi, J. W.; Cui, Y. Novel Size and Surface Oxide Effects in Silicon Nanowires as Lithium Battery Anodes. *Nano Lett.* **2011**, *11*, 4018–4025.
42. Liu, Y.; Zheng, H.; Liu, X. H.; Huang, S.; Zhu, T.; Wang, J.; Kushima, A.; Hudak, N. S.; Huang, X.; Zhang, S.; *et al*. Lithiation-Induced Embrittlement of Multiwalled Carbon Nanotubes. *ACS Nano* **2011**, *5*, 7245–7253.
43. Ghassemi, H.; Au, M.; Chen, N.; Heiden, P. A.; Yassar, R. S. *In Situ* Electrochemical Lithiation/Delithiation Observation of Individual Amorphous Si Nanorods. *ACS Nano* **2011**, *5*, 7805–7811.
44. Wang, J. W.; Liu, X. H.; Zhao, K.; Palmer, A.; Patten, E.; Burton, D.; Mao, S. X.; Suo, Z.; Huang, J. Y. Sandwich-Lithiation and Longitudinal Crack in Amorphous Silicon Coated on Carbon Nanofibers. *ACS Nano* **2012**, *6*, 9158–9167.
45. McDowell, M. T.; Lee, S. W.; Harris, J. T.; Korgel, B. A.; Wang, C.; Nix, W. D.; Cui, Y. *In Situ* TEM of Two-Phase Lithiation of Amorphous Silicon Nanospheres. *Nano Lett.* **2013**, *13*, 758–764.
46. Meunier, V.; Kephart, J.; Roland, C.; Bernholc Ab Initio Investigations of Lithium Diffusion in Carbon Nanotube Systems. *Phys. Rev. Lett.* **2002**, *88*, 075506.
47. Yang, Z.; Wu, H. Electrochemical Intercalation of Lithium into Carbon Nanotubes. *Solid State Ionics* **2001**, *143*, 173–180.
48. Datta, M. K.; Kumta, P. N. *In Situ* Electrochemical Synthesis of Lithiated Silicon-Carbon Based Composites Anode Materials for Lithium Ion Batteries. *J. Power Sources* **2009**, *194*, 1043–1052.
49. Chen, X.; Gerasopoulos, K.; Guo, J.; Brown, A.; Wang, C.; Ghodssi, R.; Culver, J. N. Virus-Enabled Silicon Anode for Lithium Ion Batteries. *ACS Nano* **2010**, *4*, 5366–5372.
50. Fong, R.; Sacken, U. von; Dahn, J. R. Studies of Lithium Intercalation into Carbons Using Nonaqueous Electrochemical Cells. *J. Electrochem. Soc.* **1990**, *137*, 2009–2013.
51. Ren, Y.; Ding, J.; Yuan, N.; Jia, S.; Qu, M.; Yu, Z. Preparation and Characterization of Silicon Monoxide/Graphite/Carbon Nanotubes Composite as Anode for Lithium-Ion Batteries. *J. Solid State Electrochem.* **2012**, *16*, 1453–1460.
52. Lee, J. I.; Choi, N. S.; Park, S. Highly Stable Si-Based Multicomponent Anodes for Practical Use in Lithium-Ion Batteries. *Energy Environ. Sci.* **2012**, *5*, 7878–7882.
53. Wang, X. L.; Han, W. Q. Graphene Enhances Li Storage Capacity of Porous Single-Crystalline Silicon Nanowires. *ACS Appl. Mater. Interfaces* **2010**, *2*, 3709–3713.
54. Ji, L.; Zhang, X. Evaluation of Si/Carbon Composite Nanofiber-Based Insertion Anodes for New-Generation Rechargeable Lithium-Ion Batteries. *Energy Environ. Sci.* **2010**, *3*, 124–129.